The Egyptian Journal of Remote Sensing and Space Sciences (2015) **18**, 261–278

HOSTED BY

ELSEVIER

National Authority for Remote Sensing and Space Sciences

The Egyptian Journal of Remote Sensing and Space Sciences

www.elsevier.com/locate/ejrs
www.sciencedirect.com

RESEARCH PAPER

Flash Flood Hazard Mapping Using Satellite Images and GIS Tools: A case study of Najran City, Kingdom of Saudi Arabia (KSA)

Ismail Elkhrachy

Najran University, Faculty of Engineering, Department of Civil Engineering, King Abdul-Aziz Rd., P.O. Box 1988, 11001 Najran, Saudi Arabia

Received 23 March 2015; revised 10 June 2015; accepted 30 June 2015
Available online 4 August 2015

KEYWORDS

DEM;
Flash flood;
ArcMap;
Flood hazard index;
Satellite image;
Remote sensing;
AHP

Abstract Flash flood in the cities led to high levels of water in the streets and roads, causing many problems such as bridge collapse, building damage and traffic problems. It is impossible to avoid risks of floods or prevent their occurrence, however it is plausible to work on the reduction of their effects and to reduce the losses which they may cause. Flash flood mapping to identify sites in high risk flood zones is one of the powerful tools for this purpose. Mapping flash flood will be beneficial to urban and infrastructure planners, risk managers and disaster response or emergency services during extreme and intense rainfall events. The objective of this paper is to generate flash flood map for Najran city, Saudi Arabia, using satellite images and GIS tools. To do so, we use SPOT and SRTM DEMs data for which accuracy assessment is achieved by using check points, obtained by GPS observations. Analytical Hierarchical Process (AHP) is used to determine relative impact weight of flood causative factors to get a composite flood hazard index (FHI). The causative factors in this study are runoff, soil type, surface slope, surface roughness, drainage density, distance to main channel and land use. All used data are finally integrated in an ArcMap to prepare a final flood hazard map for study area. The areas in high risk flood zones are obtained by overlaying the flood hazard index map with the zone boundaries layer. The affected population number and land area are determined and compared.

1. Introduction

Flash flood is generally defined as a rapid onset of flood with a short duration and a relatively high peak discharge. It occurs rapidly, generally within one hour of rainfall, and sometimes accompanied by landslides, mud flows, bridge collapse, damage to buildings, and fatalities (Hapuarachchi et al., 2011). To find some solutions to reduce the aforementioned effects, the Kingdom of Saudi Arabia (KSA), ministry of housing has offered many infrastructural and residential projects in cities in the risk of flash flood. Among these cities is Najran city, a city located in the south western of Saudi Arabia, near

E-mail address: I.Elkhrachy@yahoo.com
Peer review under responsibility of National Authority for Remote Sensing and Space Sciences.

http://dx.doi.org/10.1016/j.ejrs.2015.06.007
1110-9823

the border of Yemen. Najran extends an area of 119,000 square kilometers with a population rising from 47,500 in 1974 to 316,186 in 2013. It is of high importance for the city urban planning to map and manage the natural risk causing by flash floods for the future planning. With the advent and development of computers disaster authorities can now predict where floods will occur and how severe they're likely to be with an amazing accuracy. So far, many studies have been done to map flash flood in different countries, such as the United States (Mastin, 2009), China (Liang et al., 2011), Egypt (El Bastawesy et al., 2009; Ghoneim et al., 2002), Saudi Arabia (Saud, 2010; Dawod et al., 2011), India (Bhatt et al., 2010) and Ghana (Forkuo, 2011). Digital elevation model (DEM) is the most important input of the hydrological modeling to get Flood hazard maps. The precision of watershed calculation is directly dependent on the scale and precision of topographic maps. The difference in the scale of used maps does not only cause simplification growth of stream orders, but also cause many changes in the ration of lower order streams (El-Behiry et al., 2005). In this study, two different resolution DEMs are used one from SPOT 5 satellite and the other from Shuttle Radar Topography Mission (SRTM). Nowadays commercial remote sensing satellite sensors such as SPOT 5 panchromatic (PAN) images can be used to produce DEM for any areas on the Earth. Various applications of PAN imagery can be found in the studies of panchromatic and multispectral image fusion (Zhang, 2004) and (Simone et al., 2002), topographic mapping and digital elevation modeling (Shaker et al., 2003), feature detection and extraction(Segl and Kaufmann, 2001; Luo et al., 2007; Corbane et al., 2008), and stereo data extraction (Shaker et al., 2010). In 2003, NASA released the SRTM free data set for some regions, with 3 arc-second resolution (approximately 90 m at the equator) for the globe, and 1 arc-second (approximately 30 m at the equator) for the United States. The main purpose of the present study is to locate sites that are vulnerable to flash flood in Najran city, using a Geographical Information System (GIS) and the available data. Recently, GIS and other modern spatial techniques offer capabilities to extract drainage networks and basins that have potential to influence accumulation of run-off. Drainage flow can be integrated into the GIS program to identify areas most likely to be in the risk of flash flooding (Youssef and Pradhan, 2011).

There are many sources of errors in DEMs. Errors cover random and human error in data acquisition including errors caused by measurement equipment. They could also be due to cloud and forest cover, Earth's curvature, instable remote sensing equipment, atmospheric refraction, image processing, global positioning system (GPS) and inertial navigation system (INS) Oksanen, 2006. The mentioned errors affect the accuracy of DEM directly and hydrological modeling indirectly. Accurate DEM help to get accurate hydrological analyses and estimation of hydrographs. Assessment of how satellite derived DEM vertical inaccuracy affects watershed hydrological modeling and analysis was conducted by El Bastawesy (2007), Abou El-Magd et al. (2010), Endreny et al. (2000) and Jayaprasad et al. (2000).

In this study two DEMs, one obtained from SRTM and the other from SPOT 5 data sets, were used to analyze and calculate flow directions. SRTM DEM with 90 m resolution was downloaded from the web site (SRTM source). The primary data sets used in this study were obtained from Najran Municipality, including SPOT 5 DEM with 10 m resolution, population data of 2013 and a digital remote sensing image and zone boundaries shape file map.

2. Study area and data set

2.1. Study site

Najran city, located in the southwestern of Saudi Arabia (Fig. 1), extends between latitude of 15°–17° N and longitude 40°–45°. E. An area approximately 55 km by 28 km, characterized by moderate to high relief with elevations from 1080 m to 2252 m above mean see level (see Fig. 2). The study area is surrounded by high mountains from north, south and west. It includes various land use activities including residential, urban, and agricultural as well as road networks. Due to high elevation difference, the risk of damage caused by a flash flood is very high in this area.

2.2. Data set

Used SPOT DEM was produced by Najran Municipality with spatial resolution of 10 m. A SPOT DEM is a digital elevation model produced by automatic correlation of stereo pairs (known as Stereoscopy) acquired by the HRS instrument on SPOT 5. Stereoscopy is traditionally used to measure variation of parallax between two images of the same scene taken from different view (Anderson and Mikhail, 2001). From parallax measurement in two processing steps the DEM could be obtained. To produce DEM, the first step is to compute the parallax map and the second step is to project this map to proper coordinate system. After processing, the image is resampled to 10 m by 10 m and stored in Panchromatic (PAN) image as shown in Fig. 2a. SRTM DEM for the study area was downloaded from web site in geotiff image format, in decimal degrees and datum WGS84. The data were then projected to UTM coordinate system zone 38 N, using ArcMap (see Fig. 2b).

SRTM data cover the whole world but there are lack of data sets in some regions due to various reasons such as a lack of contrast in the radar image, presence of water, or excessive atmospheric interference. The areas, where data are missing, usually appear as holes in the maps with non-random distribution ranging from 1 pixel to regions of 500 km^2. These holes impede the potential use of SRTM data, and have been the subject of a number of innovative algorithms for filling-in the holes through various spatial analysis techniques such as interpolation methods (Reuter et al., 2007 and Jarvis et al., 2008). Information about drainage networks could be available from topographic maps, but developments in satellite image techniques provide elevation models that derive drainage networks with higher accuracy (Forte and Strobl, 2006).

It is important to examine carefully the quality of the used DEM to extract drainage network. In this work, the quality of SPOT 5 and SRTM DEMs was examined with Ground Control Points (GCPs) their elevations obtained from Global Positioning System (GPS) technique. In this study, satellite images were used after doing geometric correction to classify the study area to determine zones and constructions like buildings, roads, which may be affected during flash flood. The study area contains 75 districts as shown in Fig. 3.

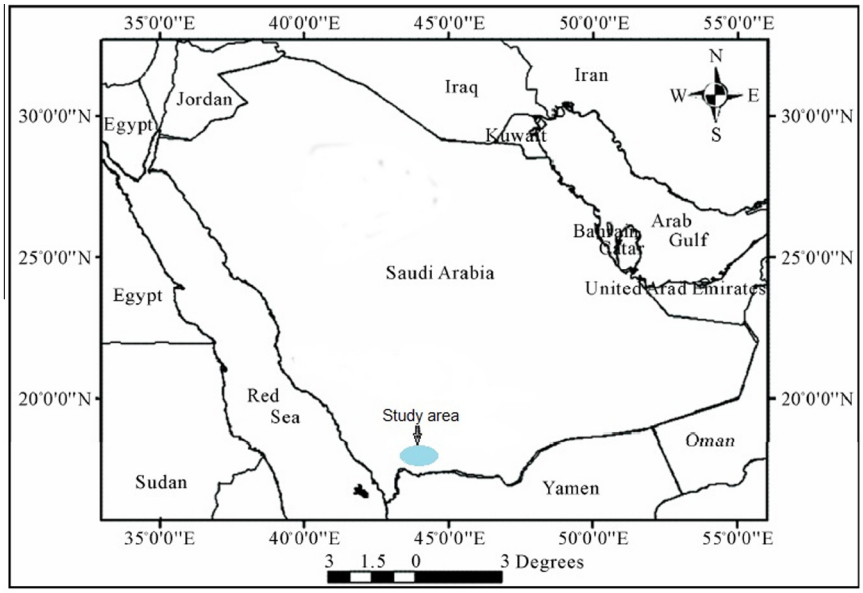

Figure 1 Geographic map of the study area (Dawod et al., 2011).

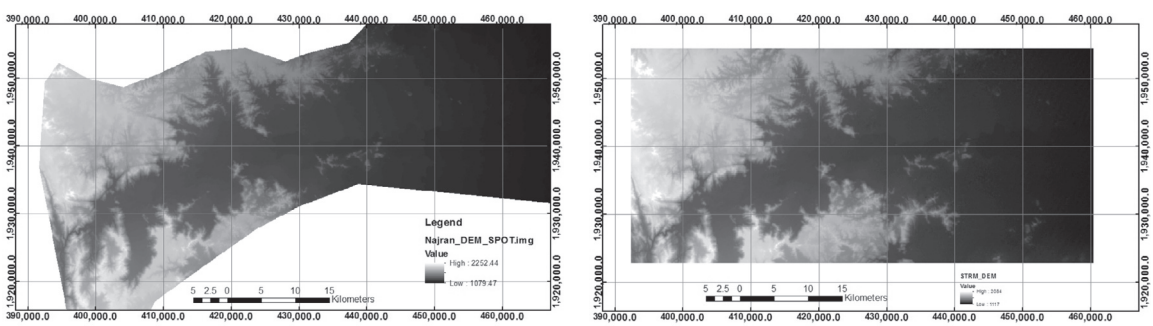

(a) SPOT 5 raw DEM (b) SRTM raw DEM

Figure 2 Raw digital elevation models of the study area; lighter areas indicate higher elevation regions. The coordinate system is UTM zone 38 north. DEM covers an area of 55 km by 28 km, with elevation ranging from 2252 to 1079 m above mean sea level.

3. Methodology

If the rainfall intensity exceeds the evaporation rate and infiltration capacity of the soil, surface runoff occurs as a flash flood. It also occurs when rainfall falls on impervious surfaces, such as roadways and other paved areas. There are many factors affecting flood hazard identification and modeling, varying from one study area to another. For instance urban flood modeling is extremely complex due to interactions with various man-made structures such as buildings, roads, culverts, channels, tunnels, and underground structures (Hapuarachchi et al., 2011). A composite flood hazard index based on seven causal factors is used during this work. These factors, which are listed here, have been elected based on different case studies with similar characteristics (Eimers et al., 2000; Yalcin and Akyurek, 2004; Pramojanee et al., 2001; El Morjani, 2011; Pedzisai, 2010 and Ho et al., 2010).

1. *Run off*: The likelihood of a flood increases as the amount of rain at a location increases (Nyarko, 2002). Higher precipitation intensity can result in more runoff because the ground cannot absorb the water quickly enough. In this study, the annual monthly maximum precipitation has been used with a return period of 14 years (see Fig. 4) to model runoff. Runoff production processes may be more important than rainfall characteristics (National Oceanic and Atmospheric Administration, 2010).
2. *Soil Influences*: Soil type and texture are very important factors in determining the water holding and infiltration characteristics of an area and consequently affect flood susceptibility (Nyarko, 2002). Some soil types can cause very rapid runoff even in dry conditions (National Oceanic and Atmospheric Administration, 2010). As a general rule, runoff from intense rainfall is likely to be more rapid and greater with clay soils than with sand.

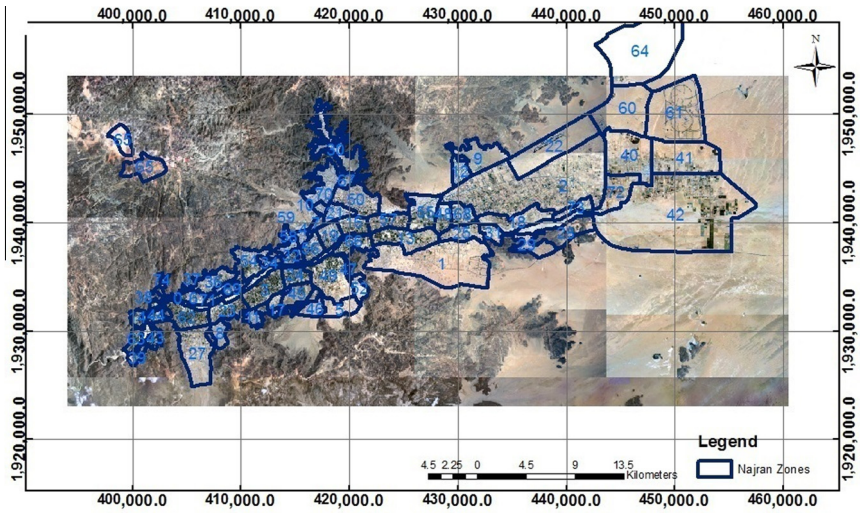

Figure 3 Worldview-2 satellite images (50 cm spatial resolution) with zone boundaries.

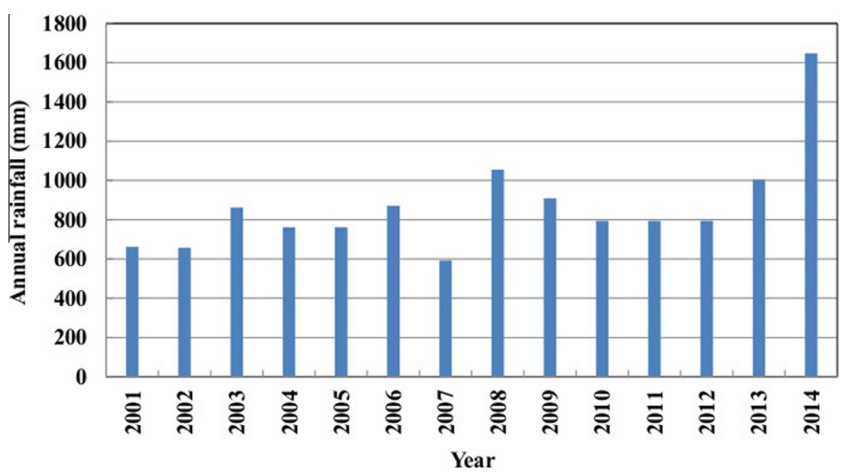

Figure 4 Annual rains in Najran city from 2000 to 2014. These data values are collected from the station located at Najran airport (http://www.theweathernetwork.com).

3. *Surface slope*: Land surface slope is one of the effective elements in floods. The danger from flash flood increases as the surface slope increases. It is a reliable indicator for flood susceptibility (Islam and Sado, 2000 and Bapalu and Sinha, 2005). When river slope increases then the flow velocity in the river also will increase (Masoudian, 2009).
4. *Surface roughness*: Surface roughness in terms of hydrodynamic friction is an essential input for flash flood simulation (National Oceanic and Atmospheric Administration, 2010). From Manning's *n* (Chow, 1959) which are empirical values. Reducing channel roughness results in faster stream flow velocities and less infiltration.
5. *Drainage density*: Drainage density is the length of all channels within the basin divided by the area of the basin. If the drainage network is dense at any area, it will be a good indicator to high flow accumulation path and more likely to get flooded (Islam and Sado, 2000).
6. *Distance to main channel*: Areas located close to the main channel and flow accumulation path are more likely to get flooded (Islam and Sado, 2000).
7. *Land cover*: This describes the appearance of the landscape and is generally classified by the amount and type of vegetation, which is a reflection of its use, environment, cultivation and seasonal phenology. Land cover is other essential influences on runoff (Alexakis et al., 2014).

Channel depth and river bed characteristic is an important factor in hydrodynamic modeling. For example, when the discharge of a river increases, the channel may become completely full. Any discharge above this level will result in the river overflowing its banks and causing a flood. But vertical resolution for used DEMs is not enough to get an accurate cross section information for delineated streams or drainage rivers. The sequences of operations are schematically shown in Fig. 5 and can be summarized as following:

1. georeferencing the satellite imagery and registering of the result to the UTM coordinate system zone 38 N. 6. doing unsupervised classification for the study area and converting population information to raster file.

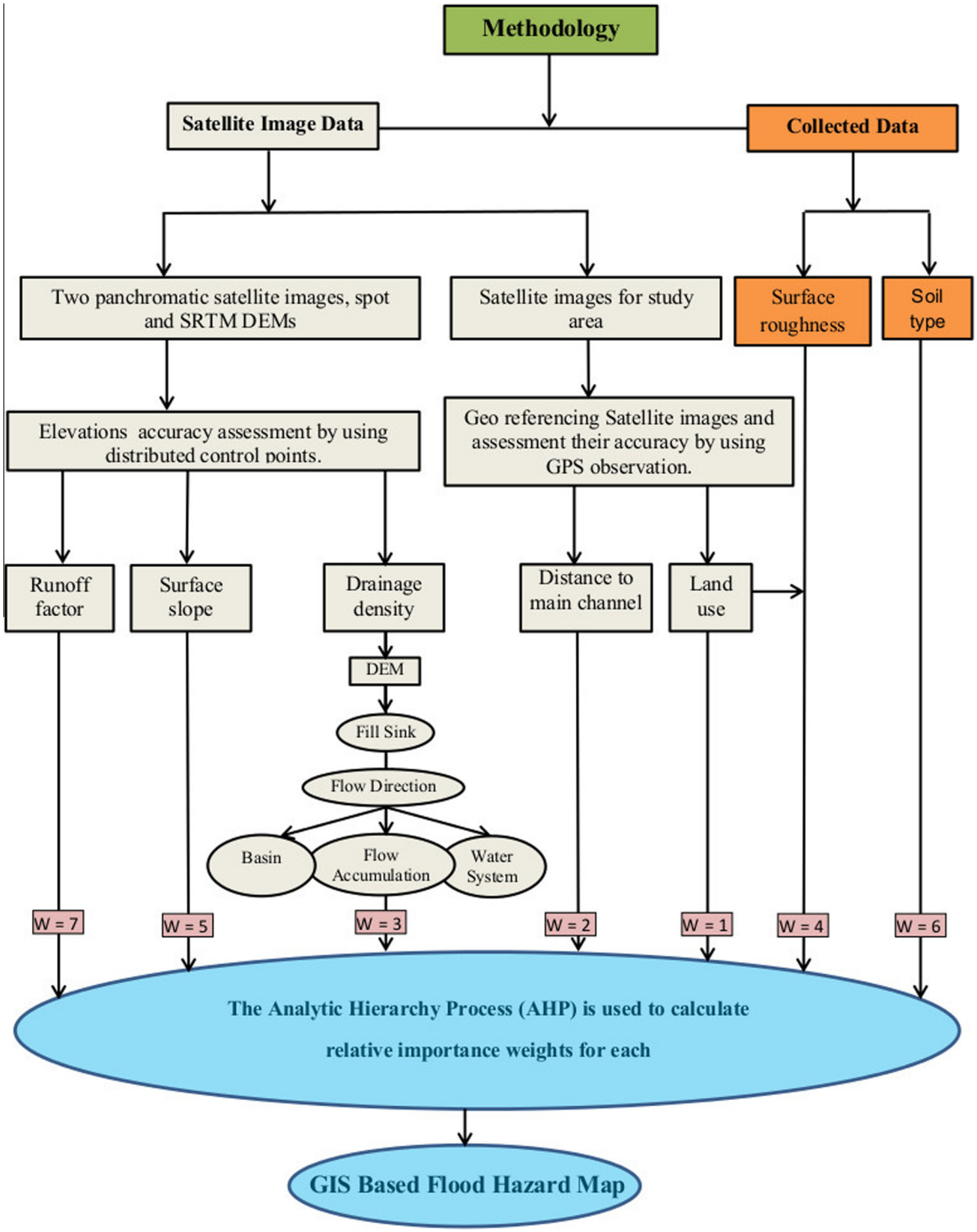

Figure 5 Methodology for flood hazard mapping (w = the weight of each flood causative factor).

2. calculating elevations accuracy for SPOT 5 and SRTM DEMs using distributed control points.
3. calculating surface slope from SPOT DEM. Slope means the maximum rate of change from every cell to its neighbors.
4. calculating drainage density from draining network and basin information.
5. extracting main channel from draining network (which has maximum stream order) followed by calculating perpendicular distance from zone centroid to main channel.
6. preparing model file by Arc Hydro and HEC-GeoHMS tools and computing hydrologic parameters by HEC-HMS software.

7. integrating all data in a GIS environment using the Analytical Hierarchical Process (AHP) method to calculate flood hazard map.

Fig. 6 shows some of data layers used in the analysis. Each is depicted in a stretch color scale, where black represents the highest values and white the lowest values. ArcMap 10.1 was used to execute the above steps for both SRTM and SPOT images to extract drainage flow net in the study area. The flow networks and basin boundaries were then vectored. The basin characteristics and the morphometric parameters were calculated from spot DEM.

AHP is a multi-criteria decision-making approach and was introduced by Masoudian (2009) and Mastin (2009). The AHP is a decision support tool. It is used to solve complex decision problems, uses a multi-level hierarchical structure of objectives, criteria, sub criteria, and alternatives. Three levels are used in our problem, Goal, factors criteria and spatial attributes. To explain The AHP, consider n elements to be compared, $C_1 \ldots C_n$ and denote the relative weight of C_i with respect to C_j by a_{ij} and form a square matrix ($A = a_{ij}$) of order n with the constraints that $a_{ij} = 1/a_{ij}$), for $i \neq j$ and $a_{ij} = 1$, all i. Such a matrix is said to be a reciprocal matrix. The weights are consistent if they are transitive, that is $a_{ik} = a_{ij}a_{ik}$ for all i, j and k. Such a matrix might exist if the a_{ij} are calculated from exactly measured data. Then find a vector ω of order n such that $A\omega = \lambda\omega$. For such a matrix, ω is said to be an eigenvector (of order n) and λ is an eigenvalue. For a consistent matrix $\lambda = n$. A Consistency Index (CI) can be calculated from $(\lambda_{max} - n)/(n - 1)$. Large samples of random matrices have been calculated by Masoudian (2009). A true Consistency ratio (Cr) is calculated by dividing the CI for the set of judgments by the Index for the corresponding random matrix. If Cr ratio exceeds 0.1 the set of judgments may be too inconsistent to be reliable. A CR of 0 means that the judgments are perfectly consistent.

4. Results and discussion

4.1. SPOT and SRTM DEM elevation accuracy assessment

Accuracy of results depends on accuracy of used digital elevation model. Vertical accuracy for two data sources of DEMs is

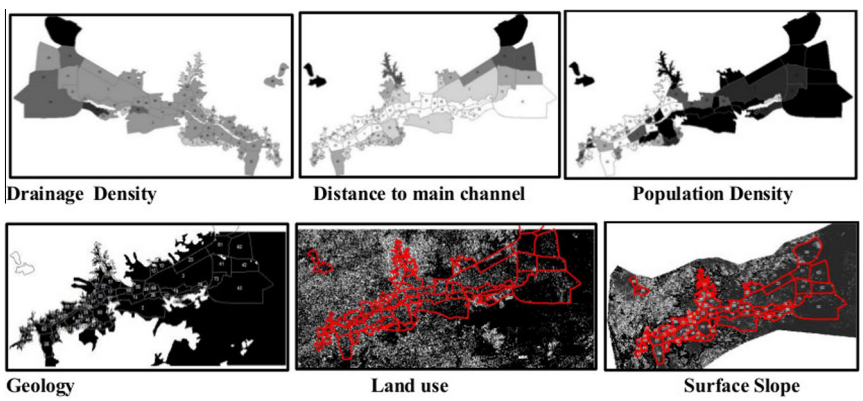

Figure 6 Some of data layers used in proposed analysis. The data are converted to raster image by using ArcMap. Darker areas indicate higher values.

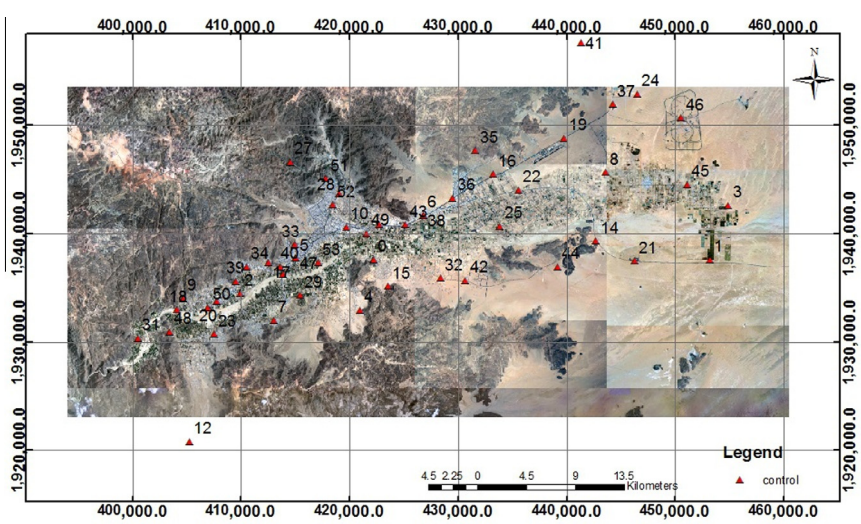

Figure 7 Ortho rectified satellite images from Worldview-2 sensor with 50 cm spatial resolution for the study area. 51 global positioning system surveyed check points are used for elevation accuracy assessment for both DEMs SPOT and SRTM .

Table 1 Summary of SPOT 5 and SRTM DEMS accuracy assessment for the study area.

Data	SPOT 5 DEM (m)	SRTM DEM (m)
Minimum	−8.61	−23.71
Maximum	29.35	25.16
Sum	−156.72	−335.55
Mean	−3.072	−6.58
Standard deviation	±5.64	±7.59

checked and compared with 51 ground control points (GCP) distributed into the study area (Fig. 7).

By using elevations of some available bench marks (BM) inside the study area, the geoid undulation N (relation between geoid and orthometric height) is calculated. The orthometric heights of GCP points are transformed. Vertical accuracy was determined by comparing the computed Z-coordinate values at check points with those obtained from post processing of GPS surveys. Statistics of the results of each DEMs are summarized in Table 1. Fig. 8 shows frequency distribution of elevation differences between 51 check points surveyed by GPS and two used DEMs. The root mean square error of elevation differences (RMSE z) for SPOT one was ±5.64 m while SRTM was found ±7.59 m.

4.2. Digital river network extraction

Digital river network from SPOT and SRTM data is extracted by using ArcMap and presented in Figs. 9 and 10. Drainage density is notably higher in SPOT data compared to the one obtained from SRTM data. Maximum river order obtained from SPOT and SRTM data sets are 7 and 6 respectively. Drainage intensity for any area is calculated by dividing summation of drainage length by the zone area as shown in Fig. 11. From this figure, the drainage network covers zones of 38, 75, 8, 14 intensely, where corresponding drainage intensity values for these zones are 34.6, 28.23, 26.56, 23.99 (km/km^2) respectively. Zone 64 has minimum intensity drainage value 0.6 (km/km^2). This indicates that zone 38 is the most likely zone that would be at the risk of flash flood.

4.3. Basin extraction

By using ArcMap, the BASIN function has been used to extract drainage basins. BASIN function analyzes the flow direction grid to find all sets of connected cells that belong to the same drainage basin. It is clear from Fig. 12 that 5 basins are covering the study area. Basin number four covers almost the whole residential area for the study area as shown in Fig. 12. Table 2 shows draining intensity for extracted basins. According to results, the study area has 5 different basins. Basin number 2 has maximum drainage intensity. Basin numbers 1 and 5 are leer from any construction like buildings or roads, numbers 2 and 3 have few of them. Residential zones for the study area lie in basin 4 as shown in Fig. 12.

4.4. Land use

Land use is the human modification of the natural environment by constructing roads or buildings, it has an effect on interception and run off velocity. Classification of satellite image means assigning corresponding levels with respect to groups with homogeneous characteristics, with the aim of discriminating multiple objects from each other within the image. The famous type of classification technique is the unsupervised classification which doesn't need prior knowledge of the area and the supervised classification which needs prior knowledge of the area (Lillesand and Kiefer, 2000). The Worldview-2 satellite images with 50 cm spatial resolution were used for classification processing. By using ArcMap 10.1, the *Iso Cluster Unsupervised classification* method is used for classification. At the beginning, twenty-five classes are chosen, finally by using Reclassify function under ArcMap toolbox, four classes were obtained: roads, building, green area and bare soil. The land cover classification map is shown in Fig. 13. Evaluation of the classification's accuracy is calculated by comparing some specific pixels of the classified image and their corresponding reference pixels, which belong to a known class, succeeds the evaluation of the classification. The results of this comparison are the error matrix, the accuracy totals and the kappa statistics (see Table 3).

4.5. Simulation of runoff using HEC-GeoHMS and HEC-HMS

The Soil Conservation Service curve number (SCS-CN) loss method is used to estimate runoff for the study area. The response of sub basin to runoff is the lag time, time from centroid of rainfall to peak runoff. This time determined by the basin shape and size, land cover soil type and topography. Only one rainfall gauge available for the whole study area is

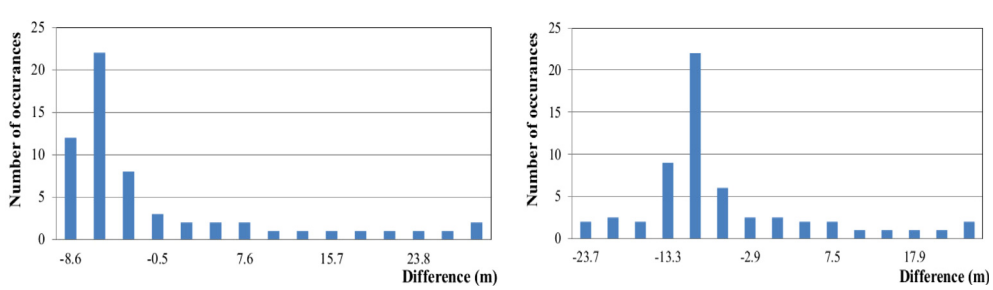

(a) SPOT 5 DEM. RMSE z = ±5.64m (b) SRTM DEM. RMSE z = ±7.58m.

Figure 8 Histogram of elevation differences between 51 check points surveyed by GPS and two used DEM s.

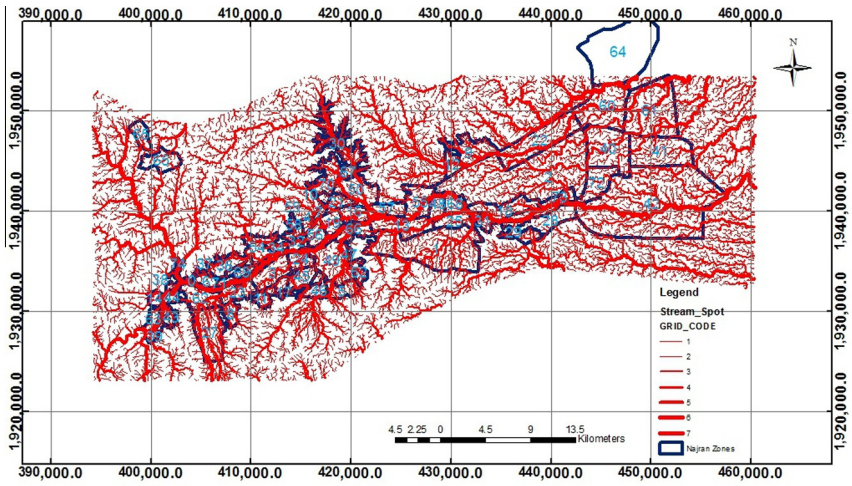

Figure 9 Najran zones and obtained drainage network from SPOT data.

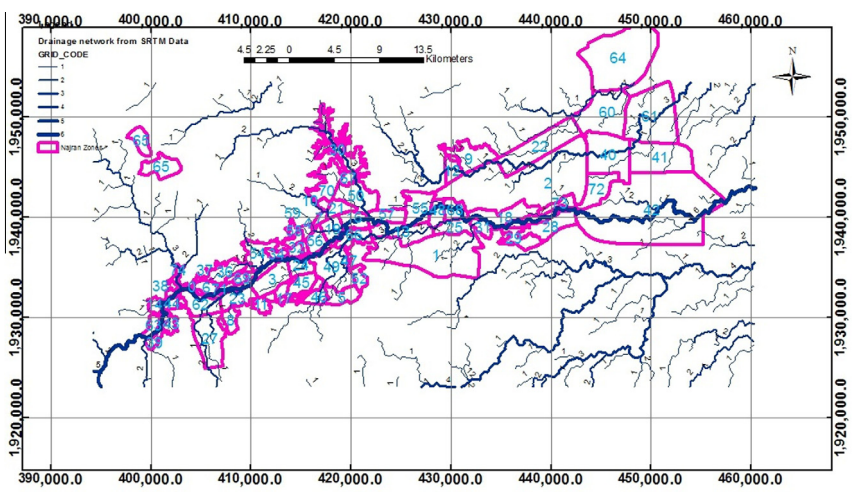

Figure 10 Najran zones and obtained drainage network from SRTM data.

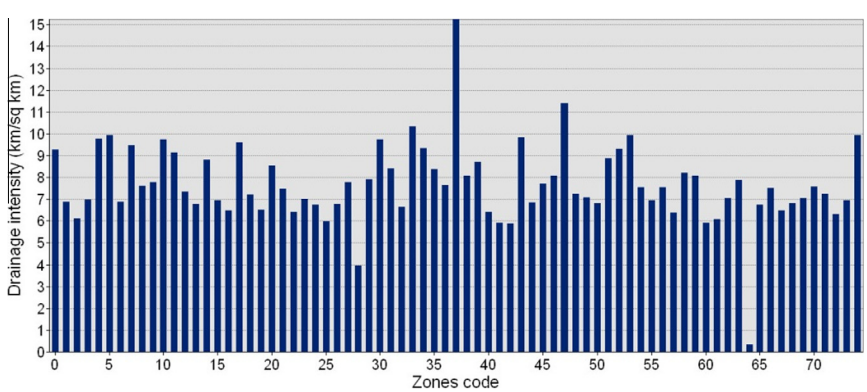

Figure 11 Drainage intensity for the study area.

used. In this study HEC-GeoHMS (US Army Corps of Engineers, 2013b) and HEC-HMS (US Army Corps of Engineers, 2013a) software are used to calculate sub basin parameters and hydrological modeling.

4.5.1. Computing sub basin parameters by using HEC-GeoHMS

By using Arc Hydro tools for ArcGIS 10.1 (ESRI, 2011), the following raster layers should be calculated for used DEM;

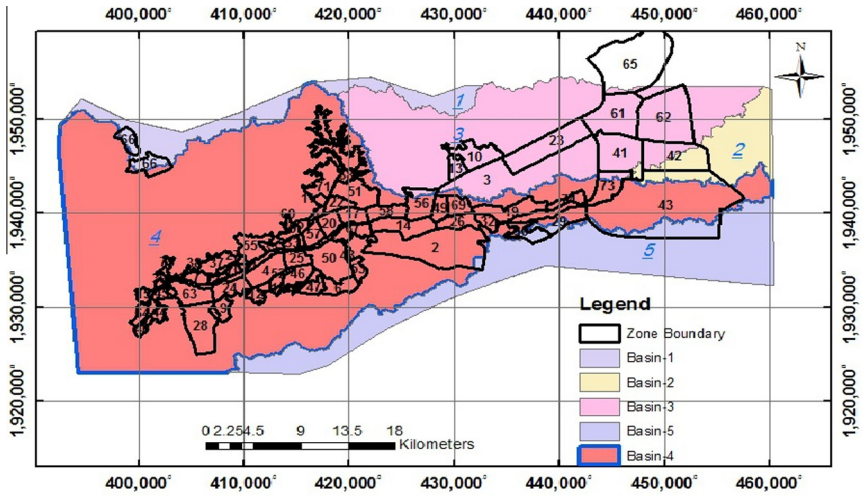

Figure 12 Najran zones and Basins extracted from SPOT data. There are five basins inside the study area. Basin number four is covering whole residential area.

Table 2 Extracted basins for the study area.

Basin nr.	Basin area km^2	Summation of network length km	Drainage intensity (km/km^2)
1	69.140	264.66	3.83
2	62.180	326.41	5.25
3	331.500	1711.44	5.16
4	929.594	4314.31	4.64
5	202.331	1023.11	5.06

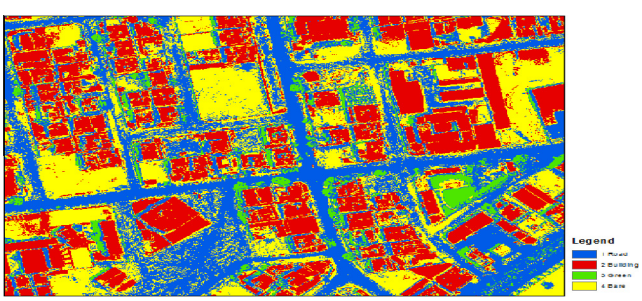

Figure 13 Unsupervised classification for the study area.

- fill sinks,
- flow direction,
- flow accumulation,
- stream definition (use threshold of 15 km^2),
- stream segmentation,
- catchment grid delineation,
- catchment polygon processing,
- drainage line processing,
- adjoin catchment processing.

HEC-GeoHMS uses ArcGIS and the Spatial Analyst extension to develop a number of hydrologic modeling. Basin number 4 contains most residential areas as shown in Fig. 12, therefore the most downstream cell of the DEM is chosen as a project point (outlet for the watershed) to generate a new project. Fig. 14 shows new project area with extracted sub basins for chosen outlet point. Longest flow length, centroid of basin, basin centroid elevation, and centroid longest flow path are calculated.

Curve number (CN) parameter is a part of calculating run-off volumes. For each sub basin, a CN value was calculated based on land use, land cover, imperviousness and hydrological soil type. Table 4 lists CNs based on combinations of Soil Conservation Service (SCS) land-use data and soil data for small urban watersheds (National engineering handbook, 1972).

To estimate the average CN values, equation 1 is used:

$$Cn_{aw} = \frac{\sum_{i=1}^{n}(Cn_i * A_i)}{\sum_{i=1}^{n} A_i} \tag{1}$$

where:

Cn_{aw} = the area weighted curve number for the drainage basin,
Cn_i = the curve number for each land use-soil group polygon,
A_i = the area for each land use-soil group polygon
n = the number of land use-soil polygon in the drainage basin.

After computing Cn grid and other hydrologic parameters HMS setting is executed. HMS setting assigns the loss method, transform method and routing method will be used in HMS and generate the HMS schematic, such as river reach, junction and sub basin.

4.5.2. Run-off model description

Lag time is defined as the length of time between the centroid of precipitation mass and the peak flow. In HEC-HMS, the parameter of lag time is necessary. The lag time was computed using the SCS lag equation. The lag time could be calculated from equation 2:

$$T_{lag} = \frac{L^{0.8}(S+1)^{0.7}}{1900(Slope)^{0.5}} \tag{2}$$

Table 3 Confusion matrix and overall accuracy and Kappa coefficient for unsupervised classification process.

	Class	Reference test information				Row total	User's Accuracy
		Road	Building	Green	Bare		
Remote sensing classificatio n	Road	101	0	25	20	146	69.18%
	Building	0	128	0	17	145	88.28%
	Green	10	0	104	1	115	90.43%
	Bare	2	4	2	105	113	92.92%
	Column total	113	132	131	143	519	
	Producer's accuracy	89.38%	96.97%	79.39%	73.43%		

Overall accuracy = 84.4%, Kappa coefficient: 0.825.

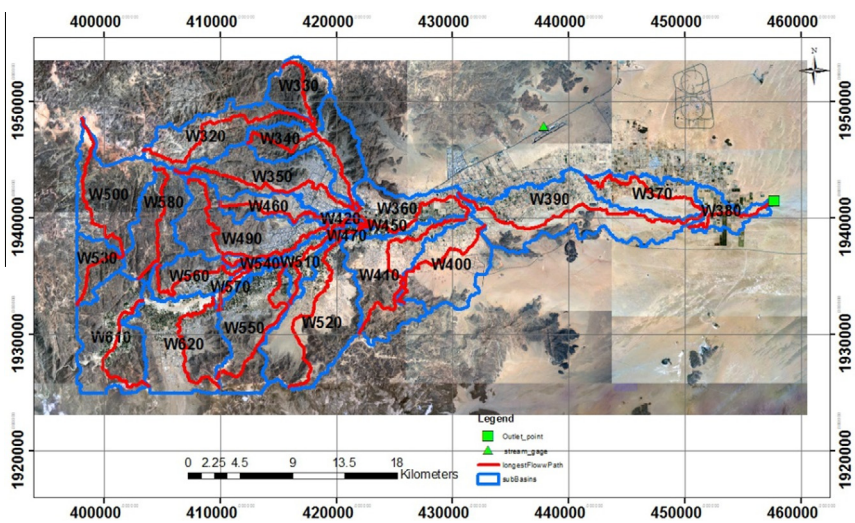

Figure 14 Automatic sub basin delineation for outlet point driven by HEC-GeoHMS based on SPOT DEM.

Table 4 Curve number generation for small urban watersheds.

SCS land use category	Hydrologic soil group			
	A	B	C	D
Road	98	98	98	98
Residential (low)	47	65	76	82
Agricultural	64	75	82	85
Bare land	77	86	91	94

Soil groups A, B, C and D are classified according to their infiltration rate.

where:

T_{lag} = lag time in hours
L = watershed length (ft)
$S = (1000/C_n) - 10$
Slope = watershed slope in percentage.

Time of concentration Tc is the longest travel time taken by a particle of water to reach a discharge point in a watershed (Wanielista et al., 1997). According to the formula proposed by SCS $T_{lag} = T_c \times 0.6$.

4.5.3. Meteorological model

The meteorological model in HEC-HMS is done by specifying a daily time series of rainfall for the month June 2008 (see Fig. 15). Rainfall data are downloaded and collected from web site http://www.theweathernetwork.com. Muskingum routing method is used.

4.5.4. Simulation results

Fig. 16 shows the summary of peak discharge and discharge volume for SCS transform method.

Table 5 presents Hydrological results in the study area. Time of concentration values varies between 20.3 and 1.0, the mean value is 5.5 h. Peak discharge values are between

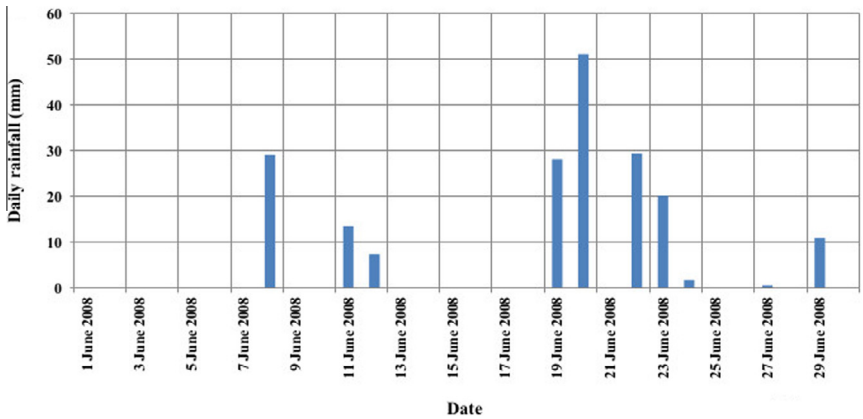

Figure 15 Rainfall information used for runoff simulation (from Jun.01.2008 to Jul.29.2008).

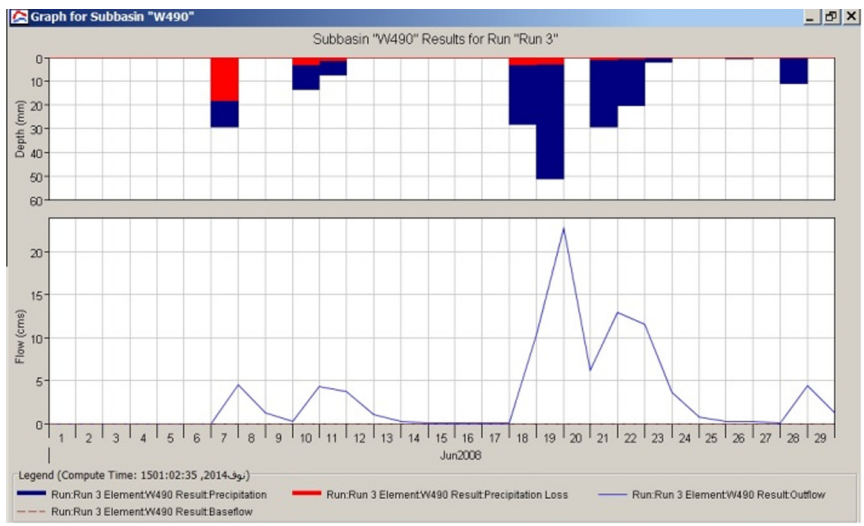

Figure 16 Runoff hydrographs from sub basin number 490.

0.1 and 22.8, mean is 10.6 m^3 /s. Surface slope values are between 1.2% and 29.3% with 14.5% mean value. Recall from Table 5, catchment 530 has the higher CN value, since it mainly has least permeability. Depending on the fact that, the lower the concentration time, the more the hazards in the runoff (Dawod et al., 2011), catchment 530 may be considered as the most hazardous catchment.

Model calibration and validation can be done by comparing model output with observed data. For the study area there are no available observed stream flows. The stream flows can be entered for a stream gauge, and linked to the watershed outlet. This helps in comparing the model output with observation, and also can be used for model calibration. The study area is suffering from absent of stream gauge data, therefore the obtained results are compared by using two different DEMs for the study area.

4.6. Estimation of the weighted scores

The objective of this research is to map flood hazard zones in Najran city. The decision factors to relate attributes to suitability concerning a particular goal are the factors controlling flood hazard in the study area. The primary decision factors are considered in this study as listed in section 3 (see Fig. 5). Once the decision factors are identified and selected, sub-factors are identified to better describe these criteria. For example, the surface slope is sub-divided into 7 sub-factors (Eimers et al., 2000) (Pramojanee et al., 2001) and (Yalcin and Akyurek, 2004). We used AHP, which is a multi-criteria decision-making approach introduced by Saaty (1977) and Saaty (1994). The AHP is a decision support tool, which is used to solve complex decision problems. It uses a multi-level hierarchical structure of objectives, criteria, sub criteria, and alternatives. Three levels are used in our problem: goal, factors criteria and spatial attributes. Each land use has a different surface roughness value. These values (ranged from 0.03 to 0.1) were specified for different land use (see Table 6).

The surface roughness map is derived from a land use map and should have the same resolution as the used DEM. In the US and Europe, a threshold in lag time of approximately 6 h is often employed to distinguish a flash flood from a slow-rising flood (Georgakakos, 1986). All causative factors are divided

Table 5 Hydrological results in the study area.

Sub basin	Area km^2	CN	Longest flow path m	T_{lag} H	T_c H	Slope%	Peak Discharge m^3/s	Volume mm
W320	38.76	90	22064.9	1.49	2.5	21.22	18.5	161.8
W330	20.40	75.63	9002.5	1.02	1.7	28.43	7.7	119.76
W340	37.29	85	17556.7	1.27	2.1	29.32	16.7	146.99
W350	45.05	90	21006.4	1.39	2.3	22.52	21.6	161.8
W360	29.85	63.26	16296.1	4.47	7.4	7.46	8	85.15
W370	26.65	55.44	16404.1	12.20	20.3	1.51	5.2	64.26
W380	13.08	55.94	10422.1	9.45	15.8	1.18	2.6	65.6
W390	66.34	58.98	28987.2	8.63	14.4	6.26	15.2	73.62
W400	40.90	58.59	15671.1	3.96	6.6	11.32	9.2	72.58
W410	48.43	66.14	22395.6	3.26	5.4	20.10	14.2	93.05
W420	3.71	62.24	5599.5	2.81	4.7	3.59	1	82.38
W450	0.37	66.95	1663.2	1.47	2.5	1.47	0.1	95.29
W460	15.01	65.36	13857.3	2.28	3.8	19.93	4.3	90.9
W470	2.06	65.08	4185.9	2.84	4.7	1.91	0.6	90.13
W490	47.61	90	22950.2	1.54	2.6	20.98	22.8	161.8
W500	43.06	90	16698.0	1.47	2.4	14.00	20.6	161.8
W510	10.87	63.34	11018.8	5.29	8.8	2.84	2.9	85.37
W520	63.97	66.14	20354.4	3.13	5.2	18.66	18.8	93.05
W530	15.70	90	7914.1	0.60	1.0	25.13	7.5	161.8
W540	4.74	63.02	7292.8	3.18	5.3	4.11	1.3	84.49
W550	44.45	71.41	18648.3	2.36	3.9	21.49	15.2	107.77
W560	21.76	68.97	14738.1	2.15	3.6	20.36	7	100.91
W570	3.96	60.52	6648.0	3.84	6.4	2.77	1	77.73
W580	35.11	75.73	13337.7	1.52	2.5	24.01	13.3	120.05
W610	49.77	85	15101.9	1.15	1.9	28.05	22.3	146.99
W620	57.13	67.18	16380.6	2.51	4.2	19.39	17.3	95.93
Total	786.03							

Table 6 Land use and surface roughness values Shaviraachin et al., (2005) and Phillips and Tadayon, (2006).

Land use	Manning's n values
Build up (buildings, houses and roads)	0.10
Bare land (sand)	0.03
Farmland (crop and paster)	0.05

into 7 sub factors to be considered in the calculation of the relative weight for each causative by using the AHP decision making approach (see Fig. 17). Pairwise comparisons are used to determine the relative importance of each alternative in terms of each criterion. Decision makers can quantify the importance of these criteria by comparing pairs of criteria on a scale of 1 to 9, from least to most important, respectively. Table 7 shows scale of relative importance to build pairwise comparison matrix (Saaty, 1977).

The weight of each factor was given on the basis of its estimated significance into cause of flooding. The weight of each factor is described in Table 8.

We also divided each factor into a number of classes and gave a weight to each class, according to its estimated significance for causing flooding. The maximum and minimum weights for each class of every factor are 7 and 1 respectively (see Fig. 17). Final weighted flood hazard index is created from an additive model which was adapted for this study (Bapalu and Sinha, 2005). RIW are the normalized eigenvectors corresponding to the maximum eigenvalues of the pair-wise comparison matrices constructed at each level of the decision hierarchy.

$$FHI = \sum_{i=1}^{n_2} (RIW_i^2) \cdot (RIW_j^2) \tag{3}$$

where:

FHI = flood hazard index.

n_2 = the number of level 2 decision factor.

RIW_i^2 = relative importance weight of level 2 decision factor i.

RIW_j^2 = relative importance weight of level 3 sub-factor j of level 2 decision factor j.

The results of pairwise comparison matrix for this work are presented in Table 9. In this table, the last column contains RIW for each criteria.

With the input values in pairwise comparison and weights calculated, consistency ratio (CR) was found to be 0.024. This indicates a reasonable level of consistency in the pairwise comparison of all factors. The FHI was used to consider the rate of probability of flooding which was calculated based on Eq. (4):

$$FHI = Rf \times 0.355 + St \times 0.240 + Slo \times 0.159 + Ro \times 0.104 + Dd \times 0.068 + Dist \times 0.045 + Lu \times 0.030 \tag{4}$$

Finally FHI is computed using weighted overlay analysis and raster calculator in ArcMap 10.1 software. The obtained values of FHI were classified into low, moderate, high and very

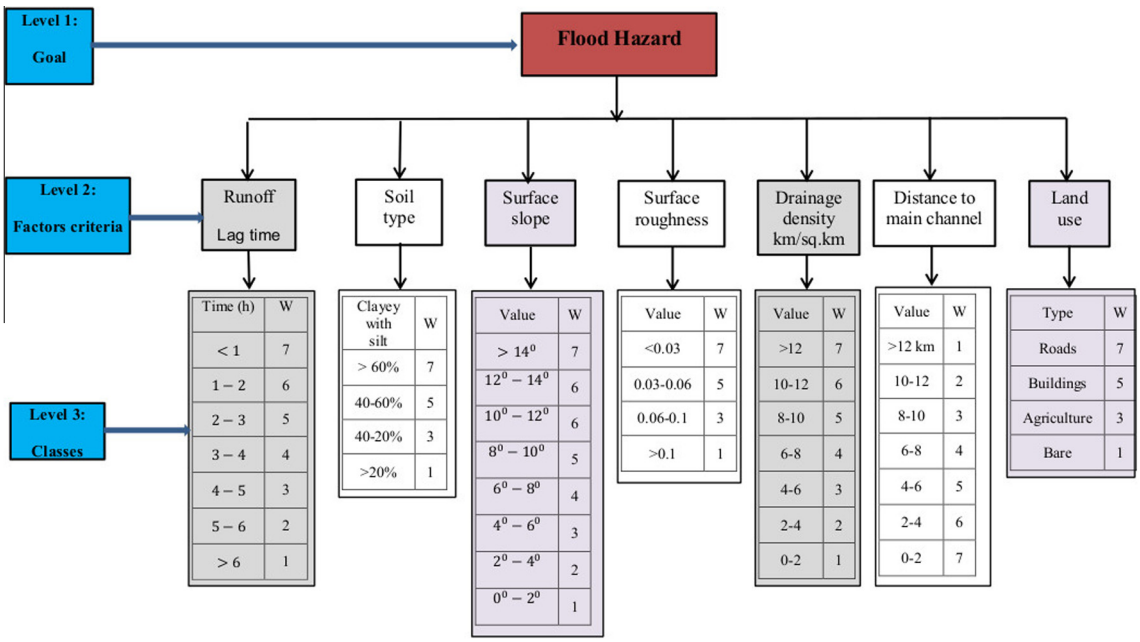

Figure 17 Decision hierarchies for flood hazard index factor.

Table 7 Scale of relative importance.

Intensity of importance Definition	Intensity of importance definition
1	Equal importance
3	Moderate
5	Strong
7	Very strong
9	Extreme importance
2,4,6 and 8	Intermediate values

Table 8 Factor weight.

Factor	Weight
Runoff	7
Soil type	6
Surface slope	5
Roughness	4
Drainage density	3
Distance to main channel	2
Land use	1

high. According to these layers and calculation the Flash Flood Hazard Map area defined is shown in Fig. 18. The natural breaks method is used for interval classification.

Hazard values have been divided into three classes. The classification scheme is summarized in Table 10. To define zones and population number likely to be affected by flash flood, zonal statistics function is used, the classification scheme is summarized in Table 10.

The areas at risk were obtained by overlaying the flood hazard index map with the zone boundaries layer. Determination of the areas at risk was needed for flood warning and floodplain development control. About 25% population residing in 17 zones is vulnerable to low, 50% population belonging to 23 zones vulnerable to moderate, 9% population belonging to 17 zones vulnerable to high and about 16% population belonging to 11 zones is vulnerable to very high flood hazard risk in the study area. The high and moderate risk areas are mostly in the relatively larger basin watersheds with high curve number, surface slope and drainage density.

Table 9 Pairwise comparison matrix and relative importance weights (RIWs) for factor criteria.

Factor criteria	Rf	St	Slo	Ro	Dd	Dist	Lu	Priority vector
Rf	1	2	3	4	5	6	7	0.355
St	0.5	1	2	3	4	5	6	0.240
Slo	0.33	0.5	1	2	3	4	5	0.159
Ro	0.25	0.33	0.50	1	2	3	4	0.104
Dd	0.20	0.25	0.33	0.5	1	2	3	0.068
Dist	0.17	0.20	0.25	0.33	0.5	1	2	0.045
Lu	0.14	0.17	0.20	0.25	0.33	0.5	1	0.030

Rf = Runoff, St = Soil type, Slo = Surface slope, Ro = Roughness, Dd = Drainage density, Dist = Distance to main channel, Lu = Land use, $\lambda_{max} = 7.196$, Cr = 0.024.

5. Effect of DEM type on flood hazard index map

DEM is the most important input of hydrological modeling. In this paper two DEMs are used to calculate some causative factors. SRTM DEM is used also to get a new flash flood hazard map for the same study area. Some of spatial maps for causative factor (which are dependent on used DEM like runoff, drainage density and surface slope) should be recalculated. Other causative factors (soil type, surface roughness, distance to main channel and land use) will remain the same for used two models, only their resolution should be adjusted to 90 m

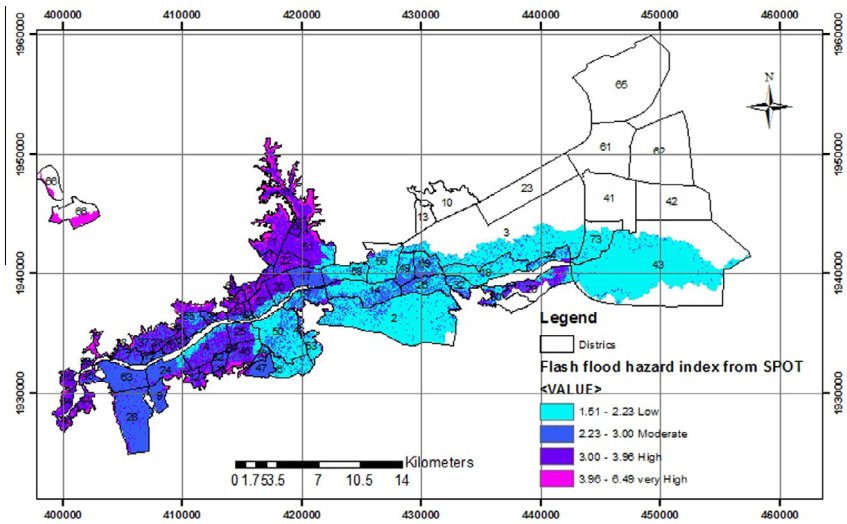

Figure 18 Flood hazard map with 10 m resolution (SPOT DEM) for the study area (each pixel has a FHI value).

Table 10 Zones and population number which may be affected by flash flood based on SPOT DEM.

FHI range	Hazard class	Number of zones likely to be affected	Total population likely to be affected	Total population (%)
4.48–3.83	Very High	11	33295	16
3.83–3.18	High	17	19233	9
3.18–2.53	Moderate	23	103295	50
2.53–1.88	Low	17	51592	25
	Total	68	207415	100

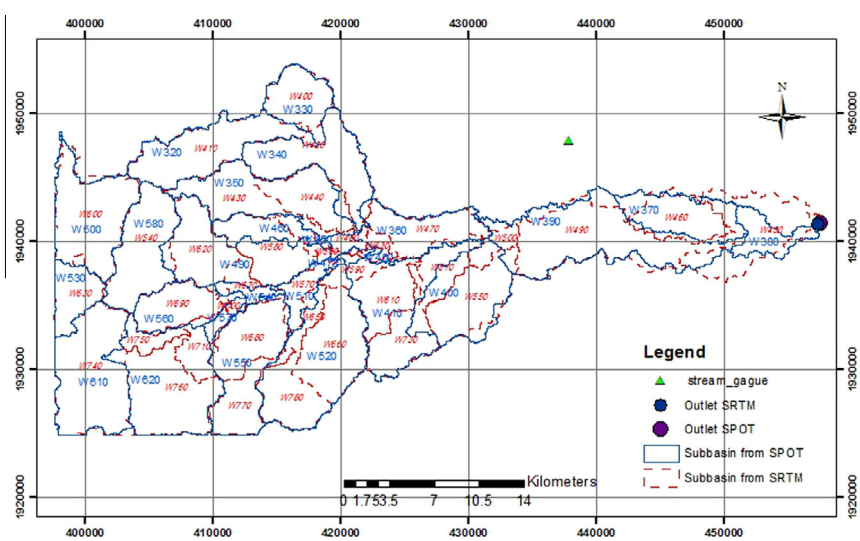

Figure 19 Automatic sub basin delineation for outlet point driven by HEC-GeoHMS by using both DEM.

instead of 10 m. A threshold value of 15 square km^2 is used in stream definition step for both used DEMs. Table 11 shows a comparison between drainage density and river lengths for both used DEMs. Maximum obtained drainage density from SPOT is almost two times than that of one SRTM.

To calculate runoff information based on SRTM DEM, HEC-GeoHMS is used to generate physical characteristics of sub basin and rivers. After that, the most downstream cell of the DEM is chosen as a project point (outlet for the watershed) to generate new project. The same storm and period

Table 11 Statistical analyses of extracted drainage length and drainage intensity for 75 zones.

Data	Drainage length		Drainage intensity	
	SPOT m	SRTM m	SPOT (km/km^2)	SRTM (km/km^2)
Minimum	0	0	0	0
Maximum	84212.8	52158.4	22.70	10.70
Sum	1092620.7	914225.5	244.14	174.10
Mean	14568.3	12188.3	3.26	2.32

information which is used before for SPOT runoff calculation is used to simulate runoff. Fig. 19 shows obtained sub basins for outlet point driven by HEC-GeoHMS from SPOT and SRTM. Some differences between sub basin boundaries from two models is noticed.

Table 12 shows Hydrological simulation results which were obtained by HEC-HMS. Time of concentration values lies between 11.82 and 1.02, mean value is 3.7 h. Peak discharge values are between 0 and 23, mean is 9.51 m^3/s. Surface slope values are between 1.04% and 21.98% with 10.27% mean value.

A new FHI is computed using weighted causative factors by using equation 4 and raster calculation in ArcMap 10.1 software. Fig. 20 shows obtained map.

To define zones and population number likely to be affected by flash flood, zonal statistics function is used. Table 13 summarizes the results.

22% population residing in 13 zones is vulnerable to low, 7% population belonging to 20 zones vulnerable to moderate, 69% population belonging to 30 zones vulnerable to high and about 2% population belonging to 5 zones is vulnerable to very high. To compare obtained results from two used DEMs, the affected area are calculated in Table 14.

The study site covers a total of 446 km^2. SPOT gives 9% of land has very high risk flooding, while SRTM gives only 3%, while obtained area with high flood risk from SRTM is doubled that one from SPOT. Low and moderate flood hazard indexes are almost the same value from both DEMs. A comparison between flash flood causative factors extracted from two DEMs is shown in Table 15. Districts 75, 31, 39, and 1 have the same value of FHI from both used DEMs.

Table 12 Hydrological results in the study area by using SRTM DEM.

Sub basin	Area km^2	CN	Longest flow path m	T_{lag} H	T_c H	Slope%	Peak Discharge m^3 /s	Volume mm
W400	19.00	83.61	7153.05	0.80	1.34	19.232	8.3	142.9
W410	37.56	84.17	19507.84	2.18	3.64	12.493	18	161.8
W420	38.70	86.95	17087.64	1.43	2.38	19.353	17.3	146.99
W430	27.61	87.88	17190.65	1.53	2.55	15.925	13.2	161.8
W440	21.38	87.72	11396.32	1.29	2.14	11.803	10.2	161.8
W450	39.15	76.79	16023.49	7.09	11.82	1.3811	15.1	123.09
W460	20.87	77.19	10843.18	5.14	8.57	1.3747	8.1	124.24
W470	22.55	78.48	13038.05	2.87	4.78	5.485	9	127.96
W480	6.96	82.51	7031.26	3.04	5.06	1.4133	3	139.68
W490	52.23	78.50	23551.55	4.98	8.29	4.6904	20.9	128.02
W500	6.86	77.68	5902.44	2.69	4.49	1.8378	2.7	125.65
W510	15.15	76.75	9220.23	4.06	6.76	1.7463	5.9	122.98
W530	4.52	73.29	4998.41	3.28	5.47	1.2211	1.6	113.09
W540	37.34	85.01	12575.03	1.35	2.25	15.237	16.7	147.01
W550	28.48	78.10	13069.71	2.30	3.84	8.7303	11.3	126.87
W560	2.02	81.43	3203.79	1.66	2.76	1.4468	0.9	136.53
W570	9.82	74.12	10126.94	4.99	8.32	1.5611	3.6	115.45
W580	26.68	85.97	11117.86	1.25	2.08	13.737	12.8	161.8
W590	8.22	77.21	8231.98	1.59	2.65	9.224	3.2	124.3
W600	42.48	83.09	15464.69	2.29	3.81	8.4718	20.3	161.8
W610	19.47	80.89	10001.93	1.37	2.28	13.571	8.2	134.95
W620	26.04	85.59	13144.27	1.36	2.27	15.495	12.5	161.8
W630	16.25	82.96	7572.06	0.95	1.59	15.712	7.8	161.8
W650	6.59	76.30	8951.45	4.10	6.83	1.6787	2.5	121.69
W660	34.17	79.64	15036.56	1.85	3.08	15.494	14	131.32
W670	10.37	80.23	7487.84	1.31	2.18	9.7936	4.3	133.03
W680	24.80	79.77	11293.31	1.73	2.88	11.106	10.2	131.7
W690	18.79	82.35	11240.20	1.29	2.16	16.685	8.1	139.21
W700	0.12	77.50	645.69	0.61	1.02	1.0352	0	125.14
W710	13.15	77.53	9876.93	1.72	2.86	10.411	5.2	125.22
W730	21.61	82.43	13510.73	1.38	2.31	19.466	9.3	139.45
W740	51.58	79.91	13920.08	1.45	2.41	21.977	23.1	146.99
W750	7.41	74.20	7737.85	2.06	3.43	5.947	2.7	115.68
W760	39.91	80.87	13748.40	1.61	2.68	16.338	16.7	134.9
W770	18.83	82.78	11565.32	1.17	1.95	20.716	8.1	140.47
W780	20.51	81.17	9401.57	1.12	1.86	18.068	8.6	135.77
Total	797.2							

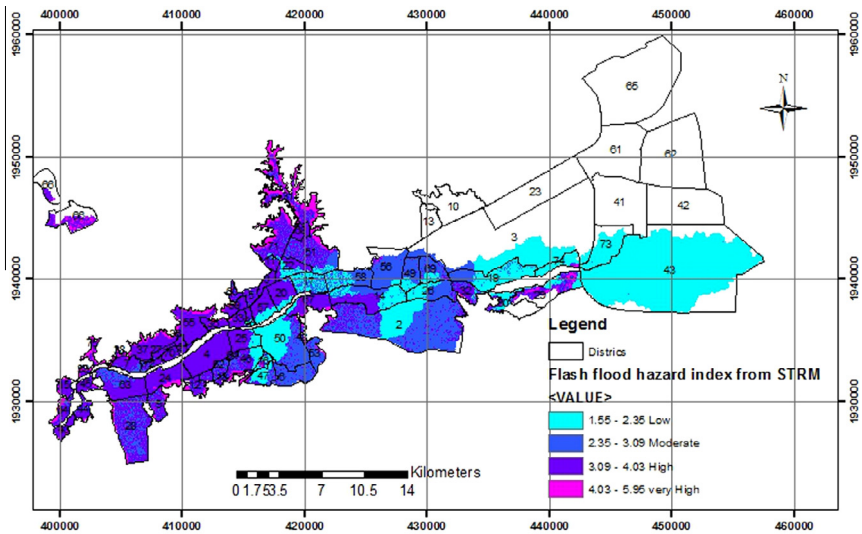

Figure 20 Flood hazard map with 90 m resolution (from SRTM DEM) for the study area (each pixel has a FHI value).

Table 13 Zones and population number which may be affected by flash flood based on SRTM model.

FHI range	Hazard class	Number of zones likely to be affected	Total population likely to be affected	Total population (%)
4.77–4.07	Very high	5	5199	2
4.04–3.31	High	30	174211	69
3.31–2.57	Moderate	20	18262	7
2.57–1.84	Low	13	55098	22
	Total	68	252770	100

Table 14 Obtained areas in different flood hazards from both DEMs.

Flood risk	SPOT DEM		SRTM DEM	
	District area likely to be affected km^2	District area (%)	District area likely to be affected km^2	District area (%)
Very high	40.6	9	13.8	3
High	44.8	10	94.8	21
Moderate	86.02	21	120.7	27
Low	274.5	62	216.7	48
Total	446	100	446	100

Table 15 Obtained areas in different flood risks from both DEMs.

Factor	SPOT			SRTM		
	Min.	Max.	Mean	Min.	Max.	Mean
Time of concentration (H)	1.02	11.82	3.7	1	20.3	5.5
Surface slope %	1.2	29.3	14.5	1.04	21.98	10.27
Districts which have very high FHI.	75, 66, 31, 40, 39, 44, 1, 15, 71, 64, 18			1, 38, 75, 39, 31		

From these results we can conclude that, low resolution DEM (SRTM) gives low surface slope and higher time of concentration for extracted basins. This explains why high resolution model (SPOT) gives more area that has very high index value (9% of total area under very high risk by using SPOT model while 3% by using SRTM). 4 districts (75, 31, 39, and 1) have the same index value from two models.

6. Conclusions and recommendations

The research presented in this article formulates an efficient methodology to accurately delineate the flood hazard areas in Najran city, KSA. Flash flood is a natural hazard that poses a risk to both populations and structures within the affected areas. There are several factors that affect the amount of run-off which help determine the intensity of flooding. Therefore, physical characteristics such as impervious surfaces, the hydraulic rating of soil, and flow accumulation of water were combined with demographic characteristics to create a composite flood hazard index. In this paper some applications of ArcMap are used to extract the drainage network based on DEM for the study area. Two DEMs (SPOT 5 and SRTM) data have been used. Accuracy assessment of used DEMs has been investigated by using check points, their elevations are collected by GPS observations. SPOT data are more accurate and dense flow network for the study area. The study area has 75 residential zones. Basin and drainage intensity of different zones is determined. The causative factors of flash flood are discussed. AHP is used to determine relative impact weight of flood causative factors to get a composite flood hazard index map. All used data are finally integrated to prepare a final

flood hazard map for the study area. By overlaying the flood hazard index map with the zone boundaries layer, the map is obtained. By using SPOT model, 25% population residing in 17 zones is prone to low flooding risk, 50% population belonging to 23 zones is prone to moderate, 9% population belonging to 17 zones is prone to high and about 16% population belonging 11 zones is prone to very high flood hazard risk. While by using SRTM model, 22% population residing in 13 zones is prone to low flooding risk, 7% population belonging to 20 zones is prone to moderate, 69% population belonging to 30 zones is prone to high and about 2% population belonging 5 zones is prone to very high flood hazard risk. Extracted flash flood causative factors (runoff, drainage density, surface slope) from low resolution DEM (SPOT) are near reality and give higher values from low one (SRTM). The sensitivity of results depends on the error in the input data as criterion weights and criterion attributes. The produced maps from the current study can be used as a guide for determining areas for further detail. Detailed flash flood hazard mapping production requires low resolution DEM which describes elevation changes densely and precisely. In the study area, the calibration of the simulation model results is difficult because of the absence of stream-gauging records. Results from both used DEMs are compared. Some recommendations can be addressed as the following:

1. Data inadequacies, stream-gauging records are absent; only one gauge for the study area is available. This leads to, flood hazard assessments based on direct measurements may not be possible.
2. The input data used in flood hazard mapping (land use and DEM maps) should be updated regularly. Updating land use maps can be done by mapping all cover changes, such as construction of dams or other major water resources projects using recently satellite images. DEM can be updated by using highly accurate and spatial resolution measurement techniques such as LiDAR, terrestrial laser scanner, total station or GPS observations.
3. Inside the study area, there are some areas that have inadequate hydraulic structures. However, the delineated boundaries are not to be taken as rigidly defining the extent of flooding. This is only possible with detailed surveys.
4. Both used DEMs are insufficient for getting accurate channel cross sections to be used for hydraulic modeling. It needs higher resolution DEM.

Acknowledgments

Author is sincerely acknowledging the data provided by Eng. Molhif Hadi Al-Haider, urban planning section, Najran Municipality, KSA. Author also thanks for technical and conceptual suggestions provided by Prof. Dr. Ahmad Helmy, Department of Civil Engineering, Najran University, KSA.

References

Abou El-Magd, I., Hermas, E.A., El Bastawesy, M., 2010. Gis-modelling of the spatial variability of flash flood hazard in Abu Dabbab catchment, Red Sea Region, Egypt. Egypt. J. Rem. Sens. Space Sci. 13, 81–88.

Alexakis, D.D., Grillakis, M.G., Koutroulis, A.G., Agapiou, A., Themistocleous, K., Tsanis, I.K., Michaelides, S., Pashiardis, S., Demetriou, C., Aristeidou, K., Retalis, A., Tymvios, F., Hadjimitsis, D.G., 2014. GIS and remote sensing techniques for the assessment of land use changes impact on flood hydrology: the case study of Yialias Basin in Cyprus. Nat. Hazards Earth Syst. Sci. 14, 413–426, URL <http://www.nat-hazards-earth-syst-sci.net/14/413/2014/nhess-14-413-2014.pdf>.

Anderson, J.M., Mikhail, E.M., 2001. In: Surveying: Theory and Practice. McGraw-Hill Company, Inc., New York, U.S.A.

Bapalu, G.V., Sinha, R., 2005. GIS in flood hazard mapping: a case study of Kosi River Basin, India. URL <http://www.gisdevelopment.net/application/natural_hazards/floods/floods001pf.htm> (accessed november 2014).

Bhatt, C.M., Rao, G.S., Manjushree, P., Bhanumurthy, V., 2010. Space based disaster management of 2008 Kosi floods, North Bihar, India. J. Indian Soc. Rem. Sens. 38 (1), 99–108.

Chow, V., 1959. Open-Channel Hydraulics, Reprint.

Corbane, C., Marre, F., Petit, M., 2008. Using spot-5hrg data in panchromatic mode for operational detection of small ships in tropical area. Sensors 8 (5), 2959–2973.

Dawod, G.M., Mirza, M.N., Al-Ghamdi, K.A., 2011. Gis-based spatial mapping of flash flood hazard in Makkah city, Saudi Arabia. J. Geogr. Inf. Syst. 11 (3), 225–231. http://dx.doi.org/10.4236/jgis.2011.33019 (URL http://www.SciRP.org/journal/jgis).

Eimers, J.L.,Weaver, J.C., Terziotti, S., Midgette, R., 2000. Methods of rating unsaturated zone and watershed characteristics of public water supplies in North Carolina. URL <http://pubs.usgs.gov/wri/wri994283/pdf/report.pdf>.

El Bastawesy, M., 2007. Influence of DEM source and resolution on the hydrographical simulation of Wadi Keed catchment, southern Sinai, Egypt. Egypt. J. Rem. Sens. Space Sci. 9, 68–79.

El Bastawesy, M., White, K., Nasr, A., 2009. Integration of remote sensing and GIS for modelling flash floods in wadi Hudain catchment. Egypt. Hydrol. Process 23 (9), 1359–1368.

El Morjani, Z., 2011. Flood hazard modelling, methodology document for the who e-atlas of disaster risk. volume 1. exposure to natural hazards version 2.0. URL <http://www.fpt.ac.ma/ Publications/Methodology_flood_hazard.pdf>. Visited on 5 October, 2014.

El-Behiry, M.G., Shided, A.A., Khadra, A.O.A, El-Huseiny, M.S., 2005. Integrated gis and remote sensing for runoff hazard analysis in Ain Sukhna industrial area, Egypt. JKAU: Earth Sci. 17, 19–42 (URL <http://www.kau.edu.sa/Files/320/Researches/51331_21521.pdf>. Visited on 2014–01–11).

Endreny, T., Wood, E., Lettenmaier, D., 2000. Satellite-derived digital elevation model accuracy: hydrogeomorphological analysis requirements. Hydrol. Process. 14, 1–20.

ESRI, 2011. Arc hydro tools - tutorial, version 2.0. URL http://downloads.esri.com/archydro/ArcHydro/Tutorial/Doc/Arc%20Hydro%20Tools%202.0%20-%20Tutorial.pdf. Visited on 23 October, 2014.

Forkuo, E.K., 2011. Flood hazard mapping using Aster Image data with GIS. Int. J. Geomat. Geosci. 1 (4).

Forte, F., Strobl, R., 2006. A methodology using GIS, aerial photos and remote sensing for loss estimation and flood vulnerability analysis in the Supersano-Ruffano-Nociglia Graben, southern Italy. Environ. Geol. 50 (4), 581–594.

Georgakakos, K.P.A., 1986. On the design of national, real-time warning systems with capability for site specific, flash-flood forecasts. Bull. Am. Meteorol. Soc. 67, 1233–1239.

Ghoneim, E.M., Arnell, N.W., Foody, G.M., 2002. Characterizing the flash flood hazards potential along the red sea coast of Egypt. The Extremes of the Extremes: Extraordinary Floods (Proceedings of a symposium held al Reykjavik. Iceland.

Hapuarachchi, H.A.P., Wang, Q.J., Pagano, T.C., 2011. A review of advances in flash flood forecasting. Hydrol. Process. 25, 2771–2784. http://dx.doi.org/10.1002/hyp.8040.

Ho, L.T.K., Umitsu, M., Yamaguchi, Y., 2010. Flood hazard mapping by satellite images and strm dem in the Vu GIA-Thu Bon Alluvial Plain, Centeral Vietnam. Int. Arch. Photogram. Rem. Sens. Spatial

Inf. Sci. 38(Part 8), 275–280 (URL <http://www.isprs.org/ proceedings/xxxviii/part8/pdf/W01OH2_20100309140832.pdf>).

Islam, M., Sado, K., 2000. Flood hazard map and land development priority map developed using AVHRR and GIS data. URL http://gisdevelopment.net/application/natural_hazards/floods/floods002pf.htm.

Jarvis, A., Reuter, H., Nelson, A., Guevara, E., 2008. Hole-filled seamless srtm data v4. International Centre for Tropical Agriculture (CIAT).

Jayaprasad, P., Nareder, B., Arya, A.S., Ajai, A., 2000. Extraction of terrain parameters from IRS-1C PAN stereo data using photogrammetric technique. Curr. Sci. 82 (3), 333–337.

Liang, W., Yongli, C., Hongquan, C., Daler, D., Jingmin, Z., Juan, Y., 2011. Flood disaster in Taihu basin, china: causal chain and policy option analyses. Environ. Earth Sci. 63 (5), 1119–1124.

Lillesand, T.M., Kiefer, R.W., 2000. Remote Sensing and Digital Image Interpretation. Wiley, New York, 724p.

Luo, J., Ming, D., Liu, W., Shen, Z., Wang, M., Sheng, H., 2007. Extraction of bridges over water from ikonos panchromatic data. Int. J. Rem. Sens. 28 (16), 3633–3648.

Masoudian, M., 2009. The topographical impact on effectiveness of flood protection measures (Ph.D. thesis). Faculty of Civil Engineering, Kassel University, Germany. URL <http://www.uni-kassel.de/upress/online/frei/978-3-89958-790-6.volltext.frei.pdf>. Visited on 2013-12-10.

Mastin, M., 2009. Watershed models for decision support for inflows to potholes reservoir, Washington.

USDA, 1972. National engineering handbook, section 4, hydrology, soil conservation service. us government printing office, Washington, dc.

National Oceanic and Atmospheric Administration, 2010. Flash flood early warning system reference guide. University corporation for atmospheric research, denver. URL http://www.meted.ucar.edu/hazwarnsys/haz_fflood.php. Visited on 12 October, 2014.

Nyarko, B.K., 2002. Application of a rational model in GIS for flood risk assessment in Accra. J. Spatial Hydrol. 2 (1), 1–14.

Oksanen, J., 2006. Digital elevation model error in terrain analysis. Ph.D. thesis, Faculty of Science, University of Helsinki. URL <http://ethesis.helsinki.fi/julkaisut/mat/maant/vk/oksanen/ digitale.pdf>. Visited on 04-06-2015.

Pedzisai, E., 2010. Rainfall-runoff modelling for flash floods in cuong think catchment; yen bai province: Vietnam. (Master thesis), International Institute for Geo-information Science and Earth Observation, Entschede, The Netherlands. URL <http://www.itc.nl/library/papers_2010/msc/aes/pedzisai.pdf>. Visited on 05-11-2014.

Phillips, J., Tadayon, S.,2006. Selection of manning's roughness coefficient for natural constructed vegetated and non vegetated channels, and vegetation maintenance plan guidelines for vegetated channels in Central Arizona. URL <http://pubs.usgs.gov/sir/2006/5108/pdf/sir20065108.pdf>.

Pramojanee, P., Tanavud, C., Yongachalermchai, C., Navanugraha, C, 2001. An application of GIS for mapping of flood hazard and risk area in Nakorn Sri Thammarat province, South of Thailand. URL <http://www.ces.iisc.ernet.in/energy/HC270799/LM/SUSLUP/Thema5/198/198.pdf>. (accessedDecember2013). (Visited on December 2013).

Reuter, H., Nelson, A., Jarvis, A., 2007. An evaluation of void filling interpolation methods for srtm data. Int. J. Geogr. Inf. Sci. 21 (9), 983–1008.

Saaty, T.L., 1977. A scaling method for priorities in hierarchical structures. J. Math. Psychol. 15, 57–68.

Saaty, T.L., 1994. Fundamentals of Decision Making and Priority Theory with the AHP. RWS Publications, Pittsburgh, PA, U.S.A.

Saud, M., 2010. Assessment of flood hazard of Jeddah area 2009, Saudi Arabia. J. Water Res. Protect. 2 (9), 839–847. http://dx.doi.org/10.4236/jwarp.2010.29099.

Segl, L., Kaufmann, H., 2001. Detection of small objects from high resolution panchromatic satellite imagery based on supervised image segmentation. IEEE Trans. Geosci. Rem. Sens. 39 (9), 2080–2083.

Shaker, A., Shi, W.Z., Emam, H., 2003. The use of empirical methods in topographic map production of irs-1dimages. The Annual Conference of American Society of Photogrammetry and Remote Sensing (May5-9, 2003).

Shaker, A., Yan, W.Y., Easa, S.M., 2010. Using stereo satellite imagery for topographic and transportation applications: an accuracy assessment. GISci. Rem. Sens. 47 (3), 321–337.

Shaviraachin, T., 2005. Flood simulation a case study in the lower limpopo vally, mozambique using the sobek flood model. Master thesis, International Institute for Geo-information Science and Earth Observation, Entschede, The Netherlands. URL <http://www.itc.nl/library/Papers_2005/msc/nrm/tumentsetseg.pdf>. Visited on 2014-03-10.

Simone, G., Farina, A., Morabito, F., Serpico, S., Bruzzone, L., 2002. Image fusion techniques for remotesensing applications. Inf. Fusion 3 (1), 3–15.

US Army Corps of Engineers, Hydrolic Engineering Center, 2013. Hec-geohms, user's manual version10.1. URL <http://www.hec.usace.army.mil/software/hec-hms/documentation/HEC-HMS_Technical%20Reference%20Manual_(CPD-74B).pdf>. Visited on 23 October, 2014.

US Army Corps of Engineers, 2013. Hydrolic Engineering Center: Hydrologic modeling system Hec-Hms, user's manual version 4. URL <http://www.hec.usace.army.mil/software/hec-geohms/downloads.aspx>. Visited on 22 October, 2014.

Wanielista M. P., K.R.E.R., 1997. Hydrology: Water Quantity and Quality Control. Wiley, New York.

Yalcin, G., Akyurek, Z., 2004. Analysing flood vulnerable areas with multicriteria evaluation. In: ISPRS Congress 2004, Istanbul, Turkey, 12-23 July. URL http://www.isprs.org/proceedings/XXXV/congress/comm2/papers/154.pdf.

Youssef, A.M., Pradhan, B., 2011. Flash flood risk estimation along the St. Katherine road, Southern Sinai, Egypt using gis based morphometry and satellite imagery. Environ. Earth Sci. 62 (3), 611–623.

Zhang, Y., 2004. Understanding image fusion. Photogram. Eng. Rem. Sens. 70(6), 657–661. http://srtm.csi.cgiar.org/SRTMdataProcessingMethodology.asp (SRTM source). http://www.theweathernetwork.com/weather/historical-weather/saudi-arabia/najran/najran?intcmp=twn_topnav_fx_historical (Rain fall information about Najran city, KSA).